

Topological Superconductivity in Multifold Fermion Metals

Jason Z. S. Gao,^{1,*} Xue-Jian Gao,^{1,*} Wen-Yu He,² Xiao Yan Xu,³ T. K. Ng,¹ and K. T. Law^{1,†}

¹*Department of Physics, Hong Kong University of Science and Technology, Clear Water Bay, Hong Kong, China*

²*Department of Physics, Massachusetts Institute of Technology, Cambridge, Massachusetts 02139, USA*

³*Department of Physics, University of California at San Diego, La Jolla, California 92093, USA*

(Dated: May 26, 2022)

Recently, two multifold fermions materials, AlPt [1] and XSi(X=Rh,Co) [2–4], characterized by multifold degeneracy band crossings at time-reversal invariant momenta (TRIMs) have been discovered in chiral crystals experimentally. In this work, we largely expand the family of multifold fermions by pointing out that several well-studied noncentrosymmetric superconductors are indeed multifold fermion metals. Importantly, their normal state topological properties, which have been ignored in previous studies, play an important role in the superconducting properties. Taking Li₂Pd₃B and Li₂Pt₃B as examples, we found a large number of unconventional degenerate point, such as double spin-1, spin-3/2, Weyl and double Weyl topological band crossing points near the Fermi energy, which result in finite Chern numbers on Fermi surfaces. Long Fermi arc states in Li₂Pd₃B, originating from the nontrivial band topology were found. Importantly, it has been shown experimentally that Li₂Pd₃B and Li₂Pt₃B are fully gapped and gapless superconductors respectively. By analyzing the possible pairing symmetries, we suggest that Li₂Pd₃B can be a DIII class topological superconductor with Majorana surface states, even if the spin-orbit coupling in Li₂Pd₃B is negligible. Interestingly, Li₂Pt₃B, being gapless, is likely to be a nodal topological superconductor with dispersion-less surface Majorana modes. We further identified that several noncentrosymmetric superconductors, such as Mo₃Al₂C, PdBiSe, Y₂C₃ and La₂C₃, are multifold fermion superconductors whose normal state topological properties have been ignored in previous experimental and theoretical studies.

Introduction.— Noncentrosymmetric superconductors are superconductors without inversion centers. The broken inversion symmetry results in antisymmetric spin-orbit coupling (ASOC) which can lead to interesting superconducting properties, such as mixed pairing order parameters [5–7], helical phases [8–10], novel magnetoelectric responses [11–14], large enhancement of the upper critical field H_{c2} [14, 15] or topological superconductivity [16–20]. In the past two decades, many noncentrosymmetric superconductors have been discovered [21]. To understand the superconducting properties of noncentrosymmetric superconductors, a common procedure was to construct normal state Hamiltonians which respect the crystal symmetry, and then to further include ASOC and study its effect on superconductivity. However, the normal state topological properties of these noncentrosymmetric superconductors have usually been ignored in previous studies.

In recent years, tremendous progress had been made in the understanding of the topological properties of band structures. Particularly, many topologically nontrivial band crossings which describe unconventional fermions, such as Weyl, Kramers Weyl and unconventional multifold fermions have been discovered [1–4, 22–25]. These multifold band crossings give rise to finite Chern numbers on Fermi surfaces enclosing the band crossing points. The case of multifold fermions is particularly interesting, as the nonsymmorphic and time-reversal symmetry can enforce multiple degeneracies and result in large Chern numbers on Fermi surfaces enclosing the band crossing points, even in the absence of ASOC. Unlike Weyl points,

which usually result in short Fermi arc states, multifold fermion crossing points result in incredibly long Fermi arc states which span a large portion of the surface Brillouin zone. So far, two multifold fermion semimetals, namely, AlPt [1] and XSi(X=Rh,Co) [2–4], have been identified, and their long Fermi arc states have been observed through ARPES experiments recently. However, they are not superconducting, and it is not known how the normal state topology resulting from multifold fermions can affect the superconducting properties in realistic materials.

In this work, we point out that Li₂Pd₃B and Li₂Pt₃B, which are well-studied noncentrosymmetric superconductors [26–29], are superconducting multifold Fermi metals and the normal state topological properties of these materials has been ignored in previous studies. Through NMR [28–30], specific heat [31, 32] and penetration length [27] measurements, it has been suggested that Li₂Pd₃B and Li₂Pt₃B are fully gapped and gapless superconductors, respectively. In the case of Li₂Pd₃B, there exist 6-fold crossings at the R-points of the Brillouin zone, and there are isolated hole pockets enclosing the R-points at the Fermi energy [29, 33]. The R-pocket carries a Chern number 4 [23], and the rest of the Fermi surfaces carry a total Chern number of -4. When the pairing of the R-pocket and the rest of the Fermi surfaces have opposite pairing signs, the material can be a fully gapped DIII class topological superconductor with four Majorana cones on the (001) surfaces. It is important to note that the finite Chern number of the R-pocket is generated by the multifold fermion which does not originate from

ASOC. This is very different from other noncentrosymmetric superconductors in which the unconventional and topological properties originate from ASOC [16–18, 34–36]. Moreover, we found long Fermi arcs on the (001) surfaces which span long distances in the surface Brillouin zone.

In the case of $\text{Li}_2\text{Pt}_3\text{B}$, the superconducting state is gapless. The order parameters belonging to both the A_1 (the isotropic representation) and A_2 representations of the O point group can result in gapless superconducting phases. Importantly, the superconducting states can be topological and possess dispersionless Majorana modes on surfaces in both A_1 and A_2 representations. Therefore, we suggest that $\text{Li}_2\text{Pt}_3\text{B}$ is a promising gapless topological superconductor candidate.

In this manuscript, we first identify topological band crossing points in $\text{Li}_2\text{Pd}_3\text{B}$ and $\text{Li}_2\text{Pt}_3\text{B}$ which are relevant to the Fermi surface topology through *ab initio* calculations. Several 2-fold, 4-fold and 6-fold band crossings which correspond to Weyl, Kramers Weyl, spin-1 and multifold fermions were found and are listed in Table I. Second, by introducing extended s-wave pairing to the bands near the Fermi energy, we show that a fully gapped DIII topological superconducting phase in $\text{Li}_2\text{Pd}_3\text{B}$ can be obtained. Four Majorana cones on the (001) surface were found. Third, we show that the gapless superconducting states of the A_1 and A_2 representations, which are relevant to $\text{Li}_2\text{Pt}_3\text{B}$, are topological and possess dispersionless Majorana surface modes. Finally, we point out that a few other well studied noncentrosymmetric superconductors, such as $\text{Mo}_3\text{Al}_2\text{C}$, PdBiSe , Y_2C_3 and La_2C_3 are also multifold fermion metals with rich topological band structures. These materials provide new platforms to study the interplay between normal state topology and superconductivity.

Multifold Fermions in $\text{Li}_2\text{Pd}_3\text{B}$ and $\text{Li}_2\text{Pt}_3\text{B}$.— Both $\text{Li}_2\text{Pd}_3\text{B}$ and $\text{Li}_2\text{Pt}_3\text{B}$ have a perovskite like cubic structure, and they belong to the nonsymmorphic space group $\text{P}4_3\text{3}2$ (No. 212) with point group O [33]. In the reciprocal space, the cubic Brillouin zone has nonequivalent high symmetry points Γ (0, 0, 0), $X(\pi/a, 0, 0)$, $M(\pi/a, \pi/a, 0)$ and $R(\pi/a, \pi/a, \pi/a)$ (with primitive lattice constant a), as shown in Fig. 2a. *Ab initio* calculations [37] are used to obtain the band structures of $\text{Li}_2\text{Pd}_3\text{B}$ and $\text{Li}_2\text{Pt}_3\text{B}$ as depicted in Fig. 1. The band structures of $\text{Li}_2\text{Pd}_3\text{B}$ and $\text{Li}_2\text{Pt}_3\text{B}$ were calculated more than a decade ago [33], but the unconventional crossing points that correspond to the multifold fermions have not been identified until recently. It was pointed out in [23] that $\text{Li}_2\text{Pd}_3\text{B}$ possesses a six-fold degenerate point at the R point even though the interplay of superconductivity and normal state topology was not studied.

To be more specific, the generators of the space group

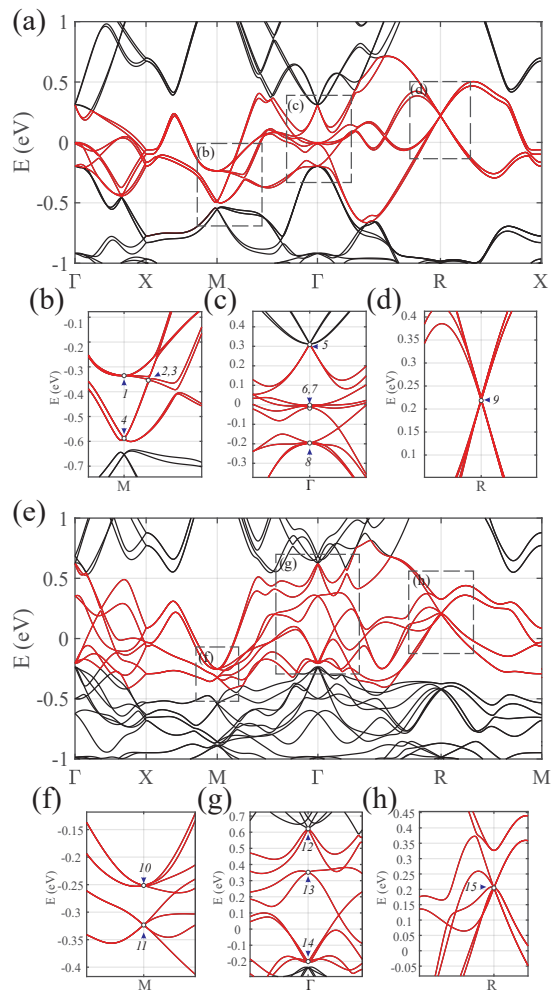


FIG. 1: (a-d) Band structure of $\text{Li}_2\text{Pd}_3\text{B}$. (e-h) Band structure of the $\text{Li}_2\text{Pt}_3\text{B}$. Bands which cross the Fermi energy are marked in red, and the topological band crossing points which can be described by unconventional fermions are depicted in enlarged plots. The degeneracies corresponding to unconventional fermions are enumerated and listed in Table I.

$\text{P}4_3\text{3}2$ (in Seitz symbols) are

$$\begin{aligned} \{2_{001}|\frac{1}{2}, 0, \frac{1}{2}\}, & \quad \{2_{010}|0, \frac{1}{2}, \frac{1}{2}\}, \\ \{3_{111}^+|0\}, & \quad \{2_{110}|\frac{1}{4}, \frac{3}{4}, \frac{1}{4}\} \end{aligned} \quad (1)$$

These crystal symmetries, together with time reversal symmetry \mathcal{T} , will stabilize a 6-fold degeneracy at Γ and 8-fold degeneracy at R in the absence of SOC. In the presence of SOC, the 6-fold symmetry will split into 4-fold and 2-fold degenerate points, while the 8-fold degeneracy at R will split into 2-fold and a 6-fold degenerate points. The effects of SOC can be seen by comparing the band structures in Fig. 1, as $\text{Li}_2\text{Pd}_3\text{B}$ has much weaker SOC than $\text{Li}_2\text{Pt}_3\text{B}$. It is important to note that the 6-fold degenerate point at R is topologically nontrivial [23]. It is described by the two spin-1 fermions, each of which gives rise to quantized Berry flux of ± 2 for a

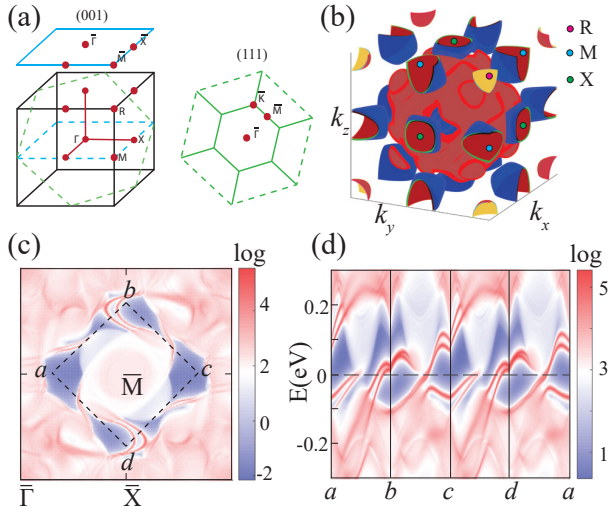


FIG. 2: (a) The bulk, the (001) surface and the (111) surface Brillouin zones of a cubic lattice. (b) The Fermi surface of $\text{Li}_2\text{Pd}_3\text{B}$. It can be seen that there are Fermi pockets enclosing all of the TRIMs. (c) Surface Fermi arcs of $\text{Li}_2\text{Pd}_3\text{B}$. The colormap represents the logarithm of spectral weight on the (001) surface. Near the Fermi energy, there are 12 Fermi arcs near the \bar{M} pocket. (d) The energy dependence of the k -points of a closed loop is indicated by dashed lines in (c). The energy spectral flow is calculated, revealing that the total topological charge of $C = 12$.

gapped surface enclosing R. Here the spin- n fermions are defined to represent the electronic states around a specific k -point that transform under the crystalline rotational symmetries in the form of $\exp(-i\hat{\mathbf{S}} \cdot \hat{\mathbf{n}}\theta)$, where $\hat{\mathbf{S}}$ is the spin- n angular momentum operator and the unit vector $\hat{\mathbf{n}}$ and θ represent the axis and angle of a rotation operation respectively. In $\text{Li}_2\text{Pd}_3\text{B}$ and $\text{Li}_2\text{Pt}_3\text{B}$, time-reversal symmetry forces two copies of spin-1 fermions to be degenerate at R [38], giving a 6-fold degeneracy as depicted in Fig. 1d. This is referred to as double spin-1 in Table I. On the other hand, the 4-fold degenerate fermions at Γ (e.g. labeled as no. 14 in Fig. 1g) are the spin-3/2 or the so-called Rarita-Schwinger-Weyl (RSW) fermions with monopole charge of ± 4 . The corresponding irreducible representations and an effective $k \cdot p$ Hamiltonian linear in k for the two aforementioned unconventional fermions are included in the Supplementary Material [37].

Kramers Weyl fermions at M , which is a TRIM, are doubled by nonsymmorphic symmetries, giving double Kramers Weyl fermions [38]. Two Weyl fermions (No. 2,3 in Table I) along the M - Γ line with a total Berry curvature charge of +2 have to be taken into account for the observed surface spectrum. For the bands which cross the Fermi energy (denoted in red in Fig. 1), 15 unconventional degenerate points are identified as unconventional chiral fermions. The locations of these points are labeled

TABLE I: Unconventional fermions found in $\text{Li}_2\text{Pd}_3\text{B}$ and $\text{Li}_2\text{Pt}_3\text{B}$ by first-principle calculation. Indices correspond to those in Fig.1.

| Type | Monopole charge | Degeneracy | No. |
|---------------------|-----------------|------------|-----------|
| Weyl | ± 1 | 2 | 2,3 |
| Kramers Weyl | ± 1 | 2 | 6,7,13 |
| Double Kramers Weyl | ± 2 | 4 | 1,4,10,11 |
| Double Spin-1 | ± 4 | 6 | 9,15 |
| Spin-3/2 | ± 4 | 4 | 5,8,12,14 |

in Fig. 1, and the degeneracy and the topological charges of the Fermi surfaces enclosing these points are summarized in Table I.

When a nondegenerate Fermi surface in the Brillouin zone encloses the band crossing points, it can acquire a finite Chern number, and there can be surface Fermi arc states connecting surfaces with different Chern numbers. The Fermi surface of $\text{Li}_2\text{Pd}_3\text{B}$ is depicted in Fig. 2b. Fig. 2c visualizes the calculated surface spectral function $\mathcal{A}_s(E, \mathbf{k}) = -\frac{1}{\pi} \text{Im} G_s(E, \mathbf{k})$ of the (001) surface of $\text{Li}_2\text{Pd}_3\text{B}$, where $G_s(E, \mathbf{k})$ is the surface Green's function. As many as 12 Fermi arcs emerge from the \bar{M} pocket. The M surface pocket is a projection of the R and M pockets of the 3D Brillouin zone, and the rest of the states enclosing the \bar{M} pocket are projections of pockets around the Γ point in the 3D Brillouin zone. The energy dispersion of the Fermi arc states are depicted in Fig. 2d. Note that all the Fermi arc states around the \bar{M} pocket have positive Fermi velocity along the a-b-c-d lines defined in Fig. 2c. This suggests that the gapped surface enclosing the M and R points in the 3D Brillouin zone has a total Chern number of 12. This is consistent with the fact that the two Fermi surfaces at the R point carry a total monopole charge of 4 and the eight Weyl points (No. 2,3 in Table I together with Weyl points related by 4-fold rotation symmetry) near M carry a total monopole charge of 8.

Pairing in superconducting $\text{Li}_2(\text{Pd}_x\text{Pt}_{1-x})_3\text{B}$.— Previous experiments have shown that $\text{Li}_2\text{Pd}_3\text{B}$ and $\text{Li}_2\text{Pt}_3\text{B}$ are superconducting with T_c at 7.5K and 2.13K , respectively [27–29]. Through NMR [28–30], specific heat and penetration depth measurements [27, 31, 32], $\text{Li}_2\text{Pd}_3\text{B}$ was found to be a fully gapped superconductor. When Pd atoms are gradually replaced by Pt atoms, the pairing gap narrows, and the material becomes gapless when $x < 0.2$ in $\text{Li}_2(\text{Pd}_x\text{Pt}_{1-x})_3\text{B}$ and remains gapless for $\text{Li}_2\text{Pt}_3\text{B}$ [29, 30]. With these exotic properties, $\text{Li}_2(\text{Pd}_x\text{Pt}_{1-x})_3\text{B}$ are promising platforms for studying the interplay between superconductivity and the topological properties of multifold fermions. However, the pairing symmetry form and the topological properties of their superconducting phases are yet to be ascertained.

In the following, we analyze the possible pairing symmetries of $\text{Li}_2(\text{Pd}_x\text{Pt}_{1-x})_3\text{B}$ from their space group

P4₃32. As inversion symmetry breaking lifts the band degeneracies at general \mathbf{k} points in the Brillouin zone except at TRIMs and Brillouin zone boundaries (due to nonsymmorphic symmetry), stable pairing on the Fermi surface is formed by the Bloch states $|\phi_{\nu,\mathbf{k}}\rangle$ and their time reversal partners $|\phi_{\nu,-\mathbf{k}}\rangle = |\mathcal{T}\phi_{\nu,\mathbf{k}}\rangle$. The pairing order parameter can be written as $\Delta_{\nu,\mathbf{k}} = \langle\phi_{\nu,\mathbf{k}}|\hat{\Delta}|\phi_{\nu,-\mathbf{k}}\rangle$ [39] as the projected pairing potential $\hat{\Delta}$ on the ν -th band. As a result, the Bogliubov-de Gennes Hamiltonian in the band basis takes the form [37]

$$\mathcal{H}_{\text{BdG}}(\mathbf{k}) = \sum_{\mathbf{k},\nu} \begin{pmatrix} \phi_{\nu,\mathbf{k}}^\dagger & \phi_{\nu,-\mathbf{k}} \end{pmatrix} \begin{pmatrix} \xi_{\nu,\mathbf{k}} & \Delta_{\nu,\mathbf{k}} \\ \Delta_{\nu,\mathbf{k}}^* & -\xi_{\nu,\mathbf{k}} \end{pmatrix} \begin{pmatrix} \phi_{\nu,\mathbf{k}} \\ \phi_{\nu,-\mathbf{k}}^\dagger \end{pmatrix}. \quad (2)$$

With the crystalline symmetry of Li₂Pd₃B and Li₂Pt₃B, the pairing $\Delta_{\nu,\mathbf{k}}$ transforms as one of the irreducible representations (IR) of the point group O, which is the factor group of P4₃32. This gives the symmetry of the pairing function, which decides the gap structure of quasi-particle spectrum [40–43]. Using this method, we can classify all the symmetry-allowed pairing functions up to their leading order in k corresponding to the irreducible representations of point group O, as listed in the supplementary Table S1 [37].

We found that the space group P4₃32 allows two one-dimensional representations, A_1 and A_2 , as listed in Table I. The A_1 representation includes the conventional s-wave and the extended s-wave pairing. As we will show below, the extended s-wave pairing can result in a fully gapped DIII class topological superconducting phase with four Majorana cones on a (001) surface. Therefore, Li₂Pd₃B can either be a fully gapped topologically trivial superconductor or a DIII class topological superconductor. For Li₂Pt₃B, with its gapless pairing, the material cannot be a fully gapped s-wave superconductor. To obtain the gapless energy spectrum, Li₂Pt₃B needs to be either in the A_2 pairing phase or in the gapless regime of the A_1 pairing phase. Importantly, both of these possible gapless pairings lead to topological phases and the surface Majorana modes. Therefore, Li₂Pt₃B is a promising gapless topological superconductor candidate. Space group P4₃32 also allows higher dimensional representations, as discussed in the Supplementary Material [37]. Nevertheless, the pairings belonging to the higher dimensional representations either break crystal symmetries or time-reversal symmetry, and the breaking of these symmetries has not been observed experimentally. Therefore, in this work, we focus on pairings associated with the one-dimensional representations.

The fully gapped A_1 pairing phase in Li₂Pd₃B.— As shown in the previous sections, the band structure of Li₂Pd₃B is highly topologically nontrivial, and the Fermi surface topological properties cannot be captured by simple effective models. Therefore, in our calculations, we first construct the Wannier orbitals from first-principle

TABLE II: Possible pairing phases of Li₂Pt₃B labeled by the 1D IR of O point group. In each IR, the pairing function $\Delta_{\nu,\mathbf{k}}$ can be expanded in terms of the basis functions. The η_ζ with $\zeta = 1, 2, 3, \dots$ there are the coefficients for the basis functions in A_1 and A_2 IR respectively.

| IR | Pairing function $\Delta_{\nu,\mathbf{k}}$ |
|-------|--|
| A_1 | $\eta_1 + \eta_2 (3 - \cos k_x a - \cos k_y a - \cos k_z a) + \dots$ |
| A_2 | $\eta_3 (\cos k_x a - \cos k_y a) (\cos k_y a - \cos k_z a) (\cos k_z a - \cos k_x a) + \dots$ |

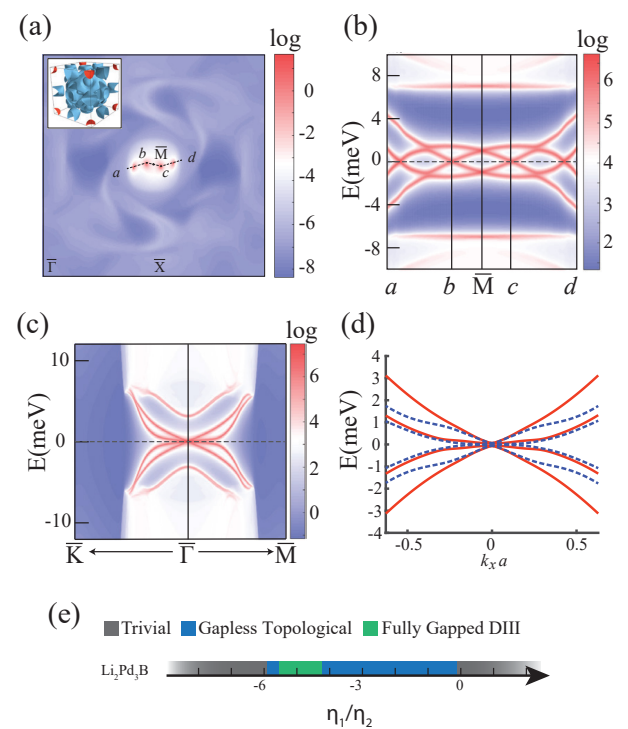


FIG. 3: (a) Four Majorana cones on the (001) surface of Li₂Pd₃B in the DIII topological phases with fully gapped A_1 pairing. The colormap represents the logarithm of quasi-particle spectral function weight on the (001) surface at $E = 0$. The inset indicates that the sign of projected pairing potential is positive (red) on the R pocket and negative (blue) on the rest. This pairing corresponds to $\eta_1/\eta_2 = -5, \eta_2 = 10$ meV, leading to an $N_{\text{gap}} = 4$ phase. (b) A zig-zag cut passing through all the Majorana cones is made and the corresponding energy spectrum is calculated. (c) and (d) show the energy spectrum of Majorana states on the (111) surface of Li₂Pd₃B in its DIII topological superconducting phase. The red solid lines and blue dashed lines in (d) represent the respective surface Majorana bands on the two sides. The different dispersion on the two sides is due to the breaking of inversion. Clearly on both (111) surface sides, there are two Majorana cones with linear and cubic dispersions. (e) Different η_1/η_2 ratios in the A_1 pairing shown in Table II give different topological superconducting phases.

calculations with the *Wannier90* package [44] and the Hamiltonian is diagonalized to obtain the eigenstates $|\phi_{\nu, \mathbf{k}}\rangle$. This allows us to incorporate the topological properties of the normal state Fermi surface when studying the superconducting phase. For simplicity, we assign the same $\Delta_{\nu, \mathbf{k}}$ to all the bands and obtain the Bogoliubov-de Gennes Hamiltonian in the form of Eq. 2. For the case of $\text{Li}_2\text{Pd}_3\text{B}$, with the A_1 representation, the superconducting properties of the system depend on η_1 and η_2 of the order parameter $\Delta_{\nu, \mathbf{k}} = \eta_1 + \eta_2 (3 - \cos k_x a - \cos k_y a - \cos k_z a)$. When $|\eta_1/\eta_2| \gg 1$, the pairing has the same sign in the whole Brillouin zone and the material is a topologically trivial superconductor. Interestingly, there is a large parameter regime, as shown Fig. 3e, that the pairing of the large Fermi pockets near Γ and the two Fermi pockets enclosing the R point have different signs. In this case, a DIII class topological superconductor is obtained [45]. The topological invariant of the DIII class topological superconductor is given by

$$N_{\text{DIII}} = \frac{1}{2} \sum_{\nu} \text{sgn}(\Delta_{\nu, \mathbf{k}_F}) C_{\nu}, \quad (3)$$

where $\Delta_{\nu, \mathbf{k}_F}$ is the pairing on the Fermi surface of the ν -th band with Chern number C_{ν} [46].

In the topological regime, as the two nearly degenerate Fermi pockets enclosing the R point have a total Chern number of 4 and the same pairing sign, and the rest of the Fermi surfaces have a total Chern number of -4 which is opposite to the R pocket, the total topological invariant of the DIII class topological phase is $N_{\text{DIII}} = 4$. As a result, we expect that four Majorana cones appear on the (001) surface of the material. This is verified numerically by setting $\eta_1/\eta_2 = -5$, so four zero energy modes are found on the Brillouin zone of the (001) surface state. It is interesting to note that on (111) surface, the C_3 rotational symmetry forces the Majorana cones to be pinned at the surface Brillouin zone center and result in two Majorana cones with linear and cubic dispersions, as shown in Fig. 3c and 3d. This cubic dispersion Majorana cone is a manifestation of the existence of multifold fermions, particularly the spin-3/2 fermions, as pointed out in [47, 48]. We would like to emphasise that the topological superconducting phase in $\text{Li}_2\text{Pd}_3\text{B}$ can be achieved with an extended s-wave pairing due to the topologically nontrivial normal state band structures. This is in sharp contrast to the DIII topological superconductors proposed in Refs. [21, 42, 47–50], which require unconventional spin-triplet pairings.

Gapless A_2 pairing in $\text{Li}_2\text{Pt}_3\text{B}$.— On the other hand, $\text{Li}_2\text{Pt}_3\text{B}$ has been experimentally found to be a gapless superconductor [27, 31, 32]. From the symmetry analysis, we note that the A_2 pairing phase with $\Delta_{\nu, \mathbf{k}} = \eta_3 (\cos k_x a - \cos k_y a) (\cos k_y a - \cos k_z a) (\cos k_z a - \cos k_x a)$ satisfies the gapless condition. It is evident from the pairing function that there are many nodal planes such as the

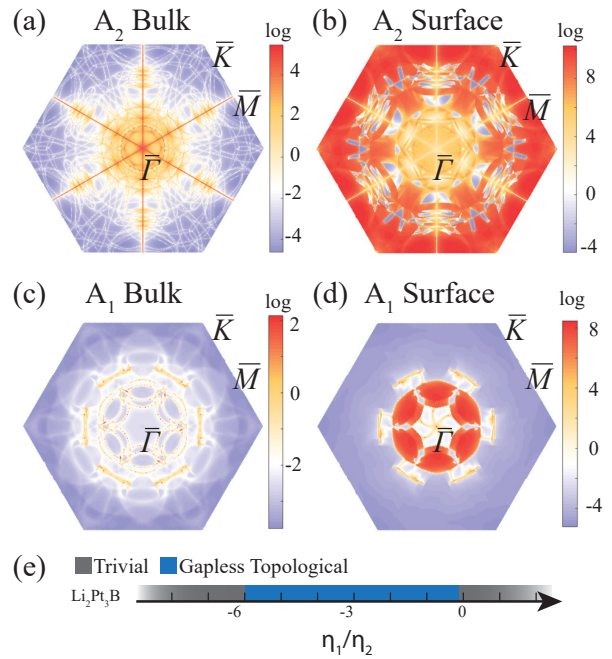


FIG. 4: Gapless topological phases of $\text{Li}_2\text{Pt}_3\text{B}$. (a) The projected bulk spectral function in the (111) direction at $E = 0$ in the A_2 phase, with $\eta_3 = 0.16\text{eV}$. (b) The surface spectral function of the (111) surface at $E = 0$ in the A_2 phase. Nodal lines shown in (a) separate the surface Majorana pockets in (b). (c) Bulk spectral functions in the A_1 phase. (d) The surface spectral function of the (111) surface in the A_1 phase. (e) The phase diagram for the A_1 phase with different η_1/η_2 .

$k_x = k_z$ plane. When the nodal planes intersect with the Fermi surface, nodal lines are formed. The projection of the nodal lines on the surface Brillouin zone can create pockets which are filled by dispersionless Majorana modes on the (111) surfaces, as shown in Fig. 4. To understand the topological origin of the dispersionless Majorana modes on the (111) surface, we can parametrize the Hamiltonian as $\mathcal{H}_{\text{BDG}}(\bar{k}_x, \bar{k}_y, \bar{k}_z)$, where \bar{k}_z is along the (111) direction and \bar{k}_x and \bar{k}_y are momenta parallel to the (111) surface. By taking \bar{k}_x and \bar{k}_y as numbers, $\mathcal{H}_{\text{BDG}}(\bar{k}_x, \bar{k}_y, \bar{k}_z)$ can be regarded as a 1D Hamiltonian $\mathcal{H}_{\text{BDG}, \bar{k}_x, \bar{k}_y}(\bar{k}_z)$ which depends on \bar{k}_z only. The topological invariant can be written as:

$$N_{\bar{k}_x, \bar{k}_y} = \frac{1}{2\pi} \text{Im} \int d\bar{k}_z \text{Tr} [\partial_{\bar{k}_z} \ln Q(\bar{k}_x, \bar{k}_y, \bar{k}_z)], \quad (4)$$

which determines the number of zero energy Majorana modes at the point (\bar{k}_x, \bar{k}_y) of the surface Brillouin zone [34, 35]. Here, $Q(\bar{k}_x, \bar{k}_y, \bar{k}_z) = H_0(\bar{k}_x, \bar{k}_y, \bar{k}_z) + i\Delta(\bar{k}_x, \bar{k}_y, \bar{k}_z)$ and $H_0(\bar{k}_x, \bar{k}_y, \bar{k}_z)$ is the normal state Hamiltonian.

It is important to note that the A_1 pairing phase can also result in a gapless spectrum. As shown in Fig. 4c and 4d, there is a wide range of parameter regime for η_1/η_2 where the system is gapless. Importantly, there are also

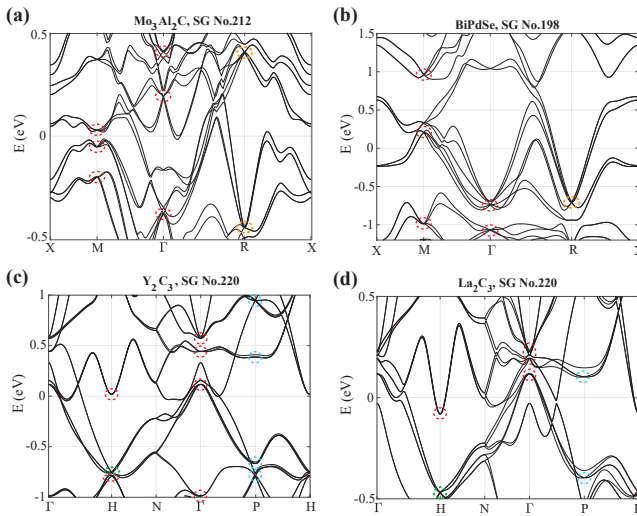


FIG. 5: The first-principle band structure of other multifold fermion superconductors, $\text{Mo}_3\text{Al}_2\text{C}$, BiPdSe , Y_2C_3 and La_2C_3 . The blue, red, orange and green dashed circles highlight the 3-, 4-, 6- and 8-fold fermions, respectively.

dispersionless surface Majorana modes on the surfaces, as shown in Fig.4d. The topological origin of the Majorana modes can also be determined by Eq. 4. Therefore, we conclude that the multifold fermion material $\text{Li}_2\text{Pt}_3\text{B}$ is likely to be a gapless topological superconductor with Majorana surface modes.

Other superconducting materials with multifold fermions.— In this work, we show that the normal state topology plays an important role in determining the superconducting properties of $\text{Li}_2\text{Pd}_3\text{B}$ and $\text{Li}_2\text{Pt}_3\text{B}$. We expect that the normal state topological properties are important in many other noncentrosymmetric superconductors as well. By revisiting the space group of noncentrosymmetric superconductors [21, 51–54], we can further identify several superconductors with multifold fermions, such as $\text{Mo}_3\text{Al}_2\text{C}$, PdBiSe , Y_2C_3 and La_2C_2 whose normal state topological properties have been ignored in previous studies. Their first-principle band structures are shown in Fig. 5. Due to their nonsymmorphic symmetries, plentiful unconventional fermions with 3-, 4-, 6- and 8-fold degeneracy appear at high-symmetry k points, and some of them are near the Fermi level and thus influence the superconducting phases. Their possible topological superconducting phases can be further studied with the same numerical and theoretical methods presented in this work.

Conclusion.— In this work, we showed that $\text{Li}_2\text{Pd}_3\text{B}$ and $\text{Li}_2\text{Pt}_3\text{B}$ are multifold fermion metals with unconventional degenerate points at time-reversal invariant momenta due to nonsymmorphic symmetry. This results in Fermi surfaces with higher Chern numbers even in the absence of ASOC. We showed that there are long Fermi

arc states in $\text{Li}_2\text{Pd}_3\text{B}$ at the Fermi energy. Interestingly, $\text{Li}_2\text{Pd}_3\text{B}$, being a fully gapped superconductor, is a candidate material of a DIII class topological superconductor. On the other hand, superconducting $\text{Li}_2\text{Pt}_3\text{B}$, being gapless, is likely to be a nodal topological superconductor with dispersionless Majorana surface modes. We also identified several other superconducting multifold fermion superconductors, which can also provide new platforms to study the interplay between normal state topology and superconductivity.

Acknowledgement.— The authors thank Mengli Hu, Ruopeng Yu and Guo-qing Zheng for valuable discussions. KTL acknowledges the support of the Croucher Foundation, the Dr. Tai-chin Lo Foundation and the HKRGC through grants C6025-19G, 16310219 and 16309718.

* These authors contributed equally to this work

† Corresponding author.
phlaw@ust.hk

- [1] N. B. M. Schroter et al., *Nat. Phys.* **15**, 759-765 (2019).
- [2] D. S. Sanchez et al., *Nature* **567**, 500-505 (2019).
- [3] Z. Rao et al., *Nature* **567**, 496-499 (2019).
- [4] D. Takane et al., *Phys. Rev. Lett.* **122**, 076402 (2019).
- [5] L. P. Gor'kov, E. I. Rashba. *Phys. Rev. Lett.* **87**, 037004 (2001).
- [6] P. A. Frigeri, D. F. Agterberg, A. Koga, and M. Sigrist. *Phys. Rev. Lett.* **92**, 097001 (2004).
- [7] P. A. Frigeri, D. F. Agterberg, and M. Sigrist. *New J. Phys.* **6**, 115 (2004).
- [8] D. F. Agterberg. *Physica C* **387**, 13–6 (2003).
- [9] R. P. Kaur, D. F. Agterberg and M. Sigrist. *Phys. Rev. Lett.* **94**, 137002 (2005).
- [10] O. V. Dimitrova and M. V. Feigel'man. *JETP Lett.* **78**, 637 (2003).
- [11] H. Mukuda, et al. *Phys. Rev. Lett.* **104**, 017003 (2010).
- [12] Yogi, Mamoru, et al. *J. Phys. Soc. J.* **75**, 013709 (2006).
- [13] Kimura, Noriaki, et al. *Phys. Rev. Lett.* **98**, 197001 (2007).
- [14] J. M. Lu et al. *Science* **350**, 1353-1357 (2015).
- [15] X. Xi et al. *Nat. Phys.* **12**, 139-143 (2016).
- [16] S. Nakosai, Y. Tanaka and N. Nagaosa. *Phys. Rev. Lett.* **108**, 147003 (2012).
- [17] M. S. Scheurer and J. Schmalian. *Nat. Commun.* **6**, 6005 (2015).
- [18] M. Sato and S. Fujimoto. *Phys. Rev. Lett.* **105**, 217001 (2010).
- [19] K. V. Samokhin. *Ann. Phys.* **359**, 385 (2015).
- [20] X. L. Qi and S. C. Zhang. *Rev. Mod. Phys.* **83**, 1057 (2011).
- [21] M. Smidman, M. B. Salamon, H. Q. Yuan, and D. F. Agterberg, *Rep. Prog. Phys.* **80**, 036501 (2017)
- [22] G. Chang et al., *Nat. Mater.* **17**, 978 (2018).
- [23] B. Bradlyn et al., *Science* **353**, 6299 (2016).
- [24] P. Tang, Q. Zhou, and S. C. Zhang, *Phys. Rev. Lett.* **119**, 206402 (2017).
- [25] G. Chang et al., *Phys. Rev. Lett.* **119**, 206401 (2017).
- [26] K. Togano, P. Badica, Y. Nakamori, S. Orimo, H. Takeya,

and K. Hirata, Phys. Rev. Lett. **93**, 247004 (2004).

[27] H. Q. Yuan, D. F. Agterberg, N. Hayashi, P. Badica, D. Vandervelde, K. Togano, M. Sigrist, and M. B. Salamon, Phys. Rev. Lett. **97**, 017006 (2006).

[28] M. Nishiyama, Y. Inada, and G. Q. Zheng, Phys. Rev. B **71**, 220505(R) (2005).

[29] M. Nishiyama, Y. Inada, and G. Zheng, Phys. Rev. Lett. **98**, 047002 (2007).

[30] S. Harada, J. J. Zhou, Y. G. Yao, Y. Inada, and G. Zheng, Phys. Rev. B **86**, 220502 (R) (2012).

[31] H. Takeya, K. Hirata, K. Yamaura, K. Togano, M. El Massalami, R. Rapp, F. A. Chaves, and B. Ouladdiaf, Phys. Rev. B **72**, 1 (2005).

[32] G. Eguchi, D. C. Peets, M. Kriener, S. Yonezawa, G. Bao, S. Harada, Y. Inada, G. Q. Zheng, and Y. Maeno, Phys. Rev. B **87**, 3 (2013).

[33] K.-W. Lee, and W. E. Pickett, Phys. Rev. B **72**, 174505 (2005).

[34] A. P. Schnyder and P. M. R. Brydon, J. Phys. Condens. Matter **27**, 243201 (2015).

[35] A. P. Schnyder, and S. Ryu, Phys. Rev. B **84**, 060504 (R) (2011).

[36] A. P. Schnyder, P. M. R. Brydon, and C. Timm. Phys. Rev. B **85**, 024522 (2012).

[37] See details in the supplementary information.

[38] C. J. Bradley, B. L. Davies. Rev. Mod. Phys. **40**, 359 (1968).

[39] A. Ramires, and M. Sigrist, Phys. Rev. B **94**, 104501 (2016).

[40] M. Sigrist and K. Ueda, Rev. Mod. Phys. **63**, 239 (1991).

[41] G. E. Volovik and L. P. Gor'kov, Zh. Eksp. Teor. Fiz. **88**: 1412-1428, (1985).

[42] J. W. F. Venderbos, L. Savary, J. Ruhman, P. A. Lee, and L. Fu, Phys. Rev. X **8**, 11029 (2018).

[43] P. M. R. Brydon, L. Wang, M. Weinert, D. F. Agterberg, Phys. Rev. Lett., **116**(17), (2016).

[44] A. A. Mostofi et al., Comput. Phys. Commun. **185**, 2309 (2014)

[45] A. P. Schnyder, S. Ryu, A. Furusaki and A.W.W. Ludwig. Phys. Rev. B **78**, 195125 (2008).

[46] X.-L. Qi, T. L. Hughes, and S.-C. Zhang, Phys. Rev. B **81**, 134508 (2010).

[47] C. Fang, B. A. Bernevig and M. J. Gilbert, Phys. Rev. B **91**, 165421 (2015).

[48] W. Yang, Y. Li, and C. Wu, Phys. Rev. Lett. **117**, 075301 (2016).

[49] L. Fu and E. Berg, Phys. Rev. Lett. **105**, 097001 (2010).

[50] M. Sato, Phys. Rev. B **81**, 220504(R) (2010).

[51] A. B. Karki, et al. Phys. Rev. B **82**, 064512 (2010).

[52] B. Joshi, et al. J. Phys.: Conf. Ser. **592**, 012069 (2015)

[53] M. C. Krupka, M. C., et al. J. Less Common Met. **17**, 91-98 (1969).

[54] A. Simon, T. Gulden, Z. Anorg. Allg. Chem. **630**, 2191–2198 (2004)